Energy Reports 4 (2018) 576–585

Contents lists available at ScienceDirect

Energy Reports

journal homepage: www.elsevier.com/locate/egyr

Research paper

A comparative study between optimal metal and composite rotors for flywheel energy storage systems

V. Kale, M. Secanell *

Energy Systems Design Laboratory, Department of Mechanical Engineering, University of Alberta, Edmonton, AB, Canada

ARTICLE INFO

Article history:
Received 8 June 2018
Received in revised form 10 September 2018
Accepted 11 September 2018
Available online 26 September 2018

Keywords:
Flywheel energy storage
Optimization
Rotor materials
Kinetic energy
Specific energy
Energy per cost

ABSTRACT

Most recent research on flywheel rotors has focused on high-speed composite rotors as the storage element of the flywheel energy storage system (FESS). Literature research indicates that this is primarily due to the high specific energy of composites compared to metals. However, a quantitative comparison of the performance of flywheels made from these materials has not been conducted. This paper aims to answer the question - 'Are composite flywheels better suited for energy storage than metal flywheels?'. This study uses three different performance indices: kinetic energy; specific energy; and, energy per cost, to compare the corresponding rotor designs. A plain-stress, linear elastic mathematical model of the flywheel rotor described by Krack et al. (2010) is used for analysis. Different optimization formulations corresponding to performance indices chosen based on the FESS application are then solved to study optimal FESS designs. The study indicates that for applications where the energy-per-cost is to be maximized, metals are superior to composite rotor materials. On a total energy basis, metals and composites are on par with each other. Composite rotors are however, superior for applications requiring high specific energy. A hybrid rotor, with a metallic energy storage element and a thin composite burst-rim, is also optimally designed and found to be a viable solution, because it offers the cost benefit of metal rotors, as well as the burst-safety provided by composites.

1. Introduction

In order to improve the reliability and robustness of the grid, short duration energy storage is of critical importance to electric utilities. Flywheels have become a feasible storage choice for typical short duration applications, such as frequency regulation (Silva-Saravia et al., 2017), voltage leveling (Cardenas et al., 2001) and fault ride-through support (Daoud et al., 2016) of intermittent sources like wind and solar farms (Arani et al., 2017). As the integration of intermittent renewable resources in the grid continues, a proportional increase in energy storage capacity will be required in order to comply with existing and future grid codes for safety, reliability and profitability. The increasing use of flywheel energy storage systems has resulted in a subsequent resurgence of research in the area of flywheel analysis and optimization in order to achieve more reliable and cost effective designs.

Some flywheel specifications for prototype storage installations across the world are listed in Table 1. The table depicts the type of flywheel rotor, power capacity, energy storage, mass, speed, self-discharge and round-trip efficiency of various manufactured flywheels. These flywheels have been installed for a variety of applications, ranging from frequency regulation, voltage support and resilience, which need short duration storage (in minutes or seconds), to reserve capacity, which needs longer duration storage (in hours). Some manufacturers have chosen to use composite rotors, while others use metal rotors. Thus, it is necessary to understand all the factors that may affect the choice of rotor material, and consequently, the optimal design and performance of the storage system.

The performance of a flywheel energy storage system (FESS) can be improved by operating it at high speeds, by choosing high strength materials, and by optimizing the shape and dimensions of the flywheel rotor (Arnold et al., 2002). The use of multiple-rim composite rotors can further increase the energy content, by optimizing the number of composite rims, the sequence of materials used in the rims, the amount of interference between the rims, and their relative thickness (Arnold et al., 2002; Genta, 2014). The properties of composite materials, such as high strength in the fiber direction, low density, and flexibility in tailoring of material properties make them a promising choice of rotor material. On the other hand, metal flywheels have advantages such as ease of manufacturing and lower cost. Standby losses occurring in FESS components, such as the bearings and electrical machine, scale with the speed of operation, thus the decreased operational speed in metal flywheels also reduces losses occurring in the system.

* Corresponding author.
E-mail address: secanell@ualberta.ca (M. Secanell).

https://doi.org/10.1016/j.egyr.2018.09.003

Table 1
Flywheel storage solutions deployed at utility scale applications.

Flywheel model	Rotor type	Power capacity kW	Energy storage kWh	Mass kg	Specific energy Wh/kg	Speed rpm	Self-discharge W	η %	Ref
Beacon Power, LLC (BP400)	Carbon composite	100	25	1133	22.06	8000–16000	4500	85	(Beacon Power Webpage, 2017)
LEVISYS	Carbon composite	10–40	10	–	–	–	–[a]	–	(LEVISYS Webpage, 2017)
Stornetic GmBH (EnWheel)	Carbon composite	22–80	3.6	–	–	<45000	–	–	(Stornetic GmBH Webpage)
Flywheel Energy Systems Inc.	Composite	50	0.75	135	5.55	15500–31000	500–1000	86	
Powerthru / Pentadyne	Carbon composite	190	0.528	590	0.89	30000–53000	250–300	–	(Powerthru Webpage, 2017)
Calnetix (VDS-XE)	4340 Aerospace steel	300	1.11	821	1.35	24500–36750	–	–	(Calnetix Webpage, 2017)
Amber Kinetcis (M32)	Low-carbon Steel	8	32	2268	14.10	<8500	65	88	(Amber Kinetics Webpage, 2017)
Temporal Power	Steel	100–500	50	3500	14.28	<10000	500	85	(Temporal Power Webpage, 2017)
ActivePower	Steel	50–250	0.958	272	3.55	7700	2500	–	(ActivePower Webpage, 2017)
ABB (PowerStore)	Steel	100–1500	5	2900	1.72	1800–3600	12000	–	(ABB Powerstore Webpage)
Piller	–	2400	5.833	–	–	1500–3600	–	–	(Piller Webpage, 2017)
Energiestro	Concrete	5	5 kWh	1700	2.94	–	–	–	(Energiestro Webpage, 2017)

[a]Three weeks standby time.

Researchers have predominantly used the specific energy as a performance measure to compare flywheel designs. Genta (2014) compared flywheel materials using their specific energy at burst speeds, which is given by the relation:

$$e = \frac{E}{m} = K\left(\frac{\sigma_u}{\rho}\right) \tag{1}$$

where e is the specific energy, E is the total energy, m is the mass of the rotor, σ_u is the ultimate strength and ρ is the density of the material. The shape factor K depends mainly on the flywheel geometry. Using Eq. (1), the specific strengths of some isotropic materials, Carbon Steel (Fe 34), Aluminium Alloy 2024, Titanium Alloy and Maraging Steel were found to be 12, 46, 63 and 66 Wh/kg respectively, and those of composites such as unidirectional Glass, Kevlar and Graphite reinforced plastics were 180, 230 and 240 Wh/kg respectively. This indicated that the theoretical maximum specific energy of composites was greater than that of metals, by a factor of 4–5 on average.

As described by Genta, however, there are some precautions to be taken when using this method to compute the specific energy. When orthotropic materials such as composites are used to fabricate flywheel rotors, the ultimate strength, σ_u, must be indicative of the failure mode of the composite rotor. Also, rotor designs with shape factors > 0.5 have bi-directional stress distributions, which cannot be handled by filament wound composite rotors with unidirectional laminates, since their tensile strengths transverse to the fiber direction (i.e., in the radial direction) are very low. Thus, designs with shape factors ≤ 0.5 must be chosen, or an alternative manufacturing method must be used, which would result in a multi-directional composite, with a better transverse tensile strength, albeit a lower hoop strength. Metal rotors, on the other hand, can be fabricated to have high shape factors, leading to improved performance. Thus, the shape factor depends on the choice of rotor material.

Liu and Jiang (2007) estimated the theoretical maximum energy density of different flywheel rotors using (1), and found the specific energy of Maraging steel, Kevlar and T700-Graphite fiber composite flywheels to be 47, 370 and 545 Wh/kg respectively, when using a fixed shape factor of 0.5, corresponding to a rotor of constant thickness. The flywheel shape used for this comparison is unfavorable for metal rotors, since they can be manufactured with complex shapes to improve the shape factor K. Bitterly (1998), calculated the specific energy of the flywheel using the relation:

$$e = 1.57E - 5\left(\frac{\sigma_\theta}{\rho}\right)\xi_{Stress}\xi_{Design} \tag{2}$$

where, σ_θ is the hoop stress, ρ is the material density, ξ_{Stress} and ξ_{Design} are safety factors for stress and design. They reported the theoretical maximum energy density e^{max} of 4340-Steel and Kevlar-49 flywheels to be 31.7 and 350 Wh/kg, using (2), with safety factors of 100% to estimate the energy density. Neither of these methods accounted for the different failure modes in composites, and thus could not be used to reliably compare the specific energy of metal and composite rotors.

Arnold et al. (2002) modified the shape factor to account for material anisotropy and stress-state multiaxiality and compared the specific energy of a slightly anisotropic and a strongly anisotropic material using the original and modified shape factors. They found that, for the strongly anisotropic material with a volume fraction of 40%, the calculated specific energy varied from 327.86 to 113.74 and to 115.36 Wh/kg when using the original 'hoop only', a modified 'radial-only' and 'multi-axial' shape factors respectively. Thus, the use of multi-axial shape factors could account for the geometry and operating conditions of the rotor more accurately. Also, this study showed that the shape factor of the type used in previous literature resulted in an over-prediction of the specific energy in the case of anisotropic materials such as composites.

The data from Table 1 indicates that there is a balanced mix of composite and metal flywheels currently being manufactured, despite evidence from previously published work that the specific energy of composites is much higher than that of metals. This leads to the following two hypotheses, which will be investigated in this paper.

The first hypothesis is that the specific energy is not the only performance index which is important while selecting the rotor material, and that there might be other factors influencing the choice of materials during the design process. In utility or grid applications, the total energy and cost might be the most important performance indices; whereas, in mobile applications, the weight or space occupied by the FESS might be a major constraint, and thus the specific energy or energy density might be the most important performance indices. There is, therefore, a need to compare optimal flywheel designs based on different criteria, depending on the application. Krack et al. (2011b,c) optimized the energy per cost of fixed volume multi-rim composite annular disk-type flywheels, by varying the operating speed and relative thickness of the composite rims, using normalized costs of rotor materials. This approach can be extended to the current work to select the best rotor materials for the optimal flywheel for the application.

The second hypothesis is that the use of a simple geometric shape factor to estimate the specific energy of a material might not accurately predict the specific energy of a rotor made of that material, especially when anisotropic materials are used. Thus, a mathematical model of the rotor is needed, which will account for material anisotropy and failure modes. When this model is used to optimize the flywheel, a more realistic value of the specific energy of the rotor can be obtained, which can then be used to choose the appropriate rotor material. An additional advantage of using an optimization formulation to determine the performance of the rotor materials is that, practical constraints other than material failure can also be checked. For example, constraints on the radial tensile stresses at the interface of multi-rim press-fitted composite rotors ensure that the composite rims do not detach due to differences in the radial expansion of the various rims.

This paper proposes to use an optimal flywheel rotor to compare and select rotor materials. The 1-D plane-stress axisymmetric

flywheel model, proposed by Krack et al. (2010) is used for the analysis. Several optimization formulations consisting of various configurations of metal and composite rotors are studied. For multiple-rim flywheels, additional interference constraints are applied, to ensure that there is no physical detachment of the rims. Comparing the optimal rotors ensures that the theoretical limits of the rotor material are reached, while also ensuring a feasible rotor design, without other failures such as detachment of press-fitted rims from the hub. Optimization objectives, such as total kinetic energy, energy per cost and specific energy are used to compare the rotors and materials. A mesh adaptive direct search (MADS) algorithm is used to solve the optimization problem, instead of the hybrid and multi-start methods employed in Krack et al. (2010). The MADS algorithm is a local, gradient-free method that has been proven to escape local minima in non-convex, non-smooth domains (Audet et al., 2008), making it more reliable than local gradient-based methods.

In Section 2, the analytical model of the flywheel is described. This model calculates the kinetic energy, stresses and deformations in the flywheel rotor at a given speed. Section 3 presents the optimization formulations, with constraints imposed on the flywheel rotor model developed in the previous section. Objectives such as kinetic energy, specific energy and energy per cost are optimized by varying the operating speed, number of rims, rim materials and relative thickness of the rims. Constraints on the material failure and rim detachment ensure that there is no failure in the flywheel. Finally, in Sections 4 and 5, the results and conclusions drawn from the studies conducted so far are presented.

2. Flywheel structural model

The flywheel mathematical model proposed by Krack et al. (2010) is used in this study. A brief overview of the model is provided below. The stored energy of the flywheel is given by

$$E = \frac{1}{2} I\omega^2 = \frac{1}{2}\rho\pi h\omega^2 \sum_{j=1}^{n}[(r_o^j)^4 - (r_i^j)^4] \tag{3}$$

where ω is the rotational speed, ρ is the density, h is the constant rotor height, n is the number of rotor rims and r_o^j, r_i^j are the outer and inner radii of the jth rim. A linear elastic model is used to determine the developed stresses in the rotor, based on the assumptions of plane stress, and axisymmetric rotation. Cylindrical coordinates are used for convenience.

2.1. Governing equations

The flywheel stresses can be found by solving Euler's equation of balance of linear momentum for a body,

$$\nabla\underline{\underline{\sigma}} + \rho\underline{b} = \rho\underline{a} \tag{4}$$

where $\underline{\underline{\sigma}}$ is the Cauchy stress tensor , $\underline{b}$ is the vector of body forces and $\underline{a}$ is the linear acceleration. The strain–displacement relation for small deformations is used, along with a linear stress–strain relation, given by Hooke's law.

$$\underline{\underline{\epsilon}} = \frac{1}{2}[\nabla\underline{u} + (\nabla\underline{u})^T] \tag{5}$$

$$\underline{\underline{\sigma}} = \underline{\underline{\underline{\underline{Q}}}}\,\underline{\underline{\epsilon}} \tag{6}$$

where $\underline{\underline{\epsilon}}$ is the strain tensor, $\underline{u}$ is the displacement vector and $\underline{\underline{\underline{\underline{Q}}}}$ is the stiffness tensor. The above relations are expressed in the cylindrical coordinate system, and the assumptions of plane stress and axisymmetry are used to obtain the second order equation:

$$\frac{\partial^2 u_r}{\partial r^2} + \frac{1}{r}\frac{\partial u_r}{\partial r} - \frac{Q_{11}}{Q_{33}}\frac{u_r}{r^2} = -\frac{\rho\omega^2}{Q_{33}}r \tag{7}$$

Here, u_r is the radial displacement, Q_{11}, Q_{33} are stiffness matrix components, ω is the operating speed and ρ is the density of the material. The derivation and solution of this equation can be found in Krack et al. (2010).

2.2. Boundary conditions

The radial stresses at the interface of the hub and the rotor, or between rims for multi-rim rotors, are continuous. Thus, the following compatibility condition is applied on the radial stresses at the interfaces:

$$\sigma_{r_i}^{j+1} = \sigma_{r_o}^{j} \tag{8}$$

where j = 1,2, …,(n - 1)

The radial displacements are continuous, but with an interference δ^j, which results from the press-fitting of the rims during assembly. This results in the displacement related compatibility condition:

$$u_{r_i}^{j+1} = u_{r_o}^{j} + \delta^j \tag{9}$$

where j = 1,2, …,(n - 1)

The stresses at the rotor outer surface are assumed to be zero. The rotor model assumes a split-type hub with negligible circumferential stress. The radial stress due to the split-type hub at the inner surface of the rotor, can be expressed using the model in Ref. (Krack et al., 2011b).

$$\sigma_{r_i}^{1} = p_i = \frac{\rho_{hub}\omega^2(r_i^3 - r_{hub}^3)}{3r_i} \tag{10}$$

$$\sigma_{r_o}^{Nrim} = 0 \tag{11}$$

2.3. Implementation

The above model is implemented and solved in Python. The numpy.linalg.solve solver, which utilizes the LAPACK routine 'dgesv', is used. The average simulation time for the analysis model is $<$ 10 ms, on a 64-bit 4-core, 3.3 GHz processor.

3. Optimization problem

3.1. Formulation

From the discussion in Section 1 it is clear that there is a need to formulate the optimization problem in a way that allows a meaningful comparison of the rotor materials. This means that the optimization formulation needs to have enough flexibility to find the true optimal rotor that can be made using any type of material. For example, the optimal composite rotor might have multiple thin rings press fitted together to form a high speed composite rotor, whereas the optimal metal rotor might be a single thick disk rotating at much lower speeds. Also, the performance index used to compare the optimal rotor materials might be different depending on the application.

In order to compare the energy content of flywheel rotors made of different materials, a rotor of the type shown in Fig. 1 is used, where the rotor height is assumed to be constant, since a thick rotor would violate the plane-stress assumption and necessitate the use of FEA simulations. The optimization problem can thus be formulated as:

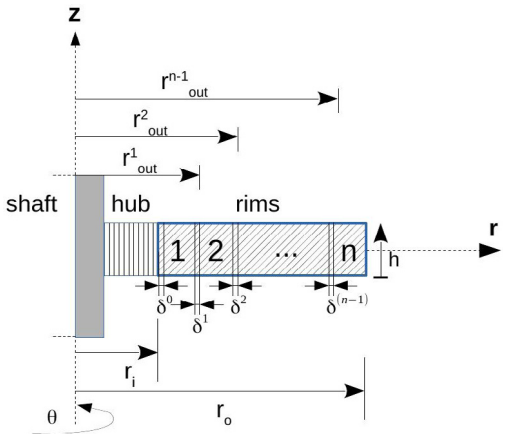

Fig. 1. Block diagram of flywheel rotor.

max: $f(\mathbf{x})$
where the objective $f(\mathbf{x})$ may be one of the following:
$\frac{1}{2}I\omega^2$, kinetic energy (KE)
$\frac{KE}{Cost}$, energy per cost
$\frac{KE}{Mass}$, specific energy
w.r.t: $\mathbf{x} = \{\omega, n, \{r^1_{out}, r^2_{out},..,r^{n-1}_{out}\},\{material_1, material_2,..,material_n\}\}$
subject to: $\frac{\sigma_i}{\sigma_i^{ult}} < 1$, material failure constraint
and $\sigma^{j+1}_{r_{in}} = \sigma^{j}_{r_{out}} \leq 0$, rim detachment failure constraint
where,
$j = 1,2,\ldots,(n-1)$; $i = (r, \theta, z)$
ω : rotor speed, rpm
n : number of rims
r^j_{out} : outer radius of rim j, m
$material_j$: material used in rim j
σ_i : stress in direction i (i = r, θ, z)
σ_i^{ult} : ultimate strength in direction i (i = r, θ, z)
$\sigma^j_{r_{in}}, \sigma^j_{r_{out}}$: radial stress at inner and outer radii of rim j.

For the material failure constraint, the yield strengths of the metals are used to compute the strength ratio for the material failure constraint, to avoid plastic deformation. For composite materials, the ultimate strengths of the composite laminates are used for their strength ratios. The maximum stress failure theory (MSFT) is used to indicate failure.

There is a constraint on the maximum radial tensile stress between the press-fitted rims of a multi-rim composite rotor. The rim detachment constraint used in this study is a novel one, which can allow the optimization routine to yield better results than in the past. Previous research conducting optimization of press-fitted multi-rim flywheels used a constraint which restricted the radial stresses in the flywheel to compressive (negative) values at all points along the radius (Krack et al., 2011b). The new rim-detachment constraint only restricts the radial stresses to compressive values at the interface between rims, where the load cannot be transferred in the radial direction. Thus, other regions in the flywheel may be subjected to radial tensile stresses within the material elastic limits, which further increases the energy capacity of the optimal FESS. The number of rims in multi-rim composite rotors has been limited to two in this study, since it has been demonstrated by previous researchers (Ertz, 2014; Krack et al., 2011a), that a further increase in the number of rims results in a limited improvement in the performance of the flywheel.

3.2. Implementation

The optimization problem is solved using DAKOTA toolbox (Adam et al., 2015), which allows the use of its optimization algorithms as a black box, using a script interface. A schematic of the interface between DAKOTA, and the analysis code, implemented in Python is shown in Fig. 2. A MADS algorithm is used to solve this non-linear constrained optimization problem, as it is a local, gradient free method, and is more reliable than local gradient-based methods, while being faster than global methods such as genetic algorithms. It also has minimal dependence on the initial guess of the design variables. This method has been shown to reliably solve non-convex problems, which can prove challenging for gradient-based methods because of their tendency to get stuck in local optima when the optimization problem is non-convex (Audet et al., 2008).

The MADS algorithm is a direct search method, which evaluates the optimization responses at a set of trial points lying on a discrete mesh. Each iteration consists of three steps—poll, search and update. The poll and search steps both generate trial points on the mesh. The search step can generate trial points anywhere on the mesh, and can be tailored by a user-defined strategy such as the variable neighborhood search, whereas the poll step creates trial points that are bounded by the distance from the current poll center as well as a set of poll directions. The responses at all the trial points are evaluated, and based on the failure or success of the evaluation, determined in the update step, the mesh is either refined or coarsened. The 'threshold delta' parameter, which defines the minimum mesh size, the 'function precision' parameter, which defines the resolution of the objectives and constraints and the 'maximum number of black-box evaluations' parameter are the termination criteria in this method. The 'variable neighborhood search' parameter denotes the percentage of evaluations used to escape local minima and converge to a globally optimal solution.

3.3. Model validation

The flywheel mathematical model used in this study was validated against the results published by Krack et al. (2010). A 2-rim composite rotor consisting of an inner glass-epoxy rim and an outer carbon-epoxy rim was simulated. The composite material properties and flywheel dimensions from Krack et al. (2010) were used. The radial and hoop stresses developed in the flywheel rotating at 30,000 rpm were then plotted, and compared with the stresses developed in a single rim rotor made from either of the 2 composite materials. It was found that the radial stresses developed in the rotor were reduced by introducing an extra rim. The stress distributions in the 1-rim and 2-rim composite flywheel rotors, obtained from the Python model described in Section 2 are shown in Fig. 3. The results were in agreement with the previous publication.

In order to validate the optimization framework, the design problem in Krack et al. (2010) was also solved. The energy per unit cost of materials, for the 2-rim glass-epoxy and carbon-epoxy composite flywheel, was maximized by varying the operating speed and the relative thickness of the 2 composite rims. The optimal solution was obtained for 4 different cost ratios of the materials used in the rims. Table 2 shows a comparison of the optimal solution with the proposed framework and the solution obtained in Krack et al. (2010). The simulated results were within $\pm 0.3\%$ of the literature results, which could be due to the use of different optimization algorithms.

The proposed optimization formulation discussed in Section 3, introduced an additional constraint on the radial stress developed at the interface of press-fit rims in multi-rim rotors. This constraint was necessary to ensure that there are no radial tensile stresses at the rim interfaces, which could result in failure due to detachment of the rims. The necessity and significance of this new constraint was investigated. This constraint was not used in Krack et al. (2010) because the radial stress at the rim interface became more

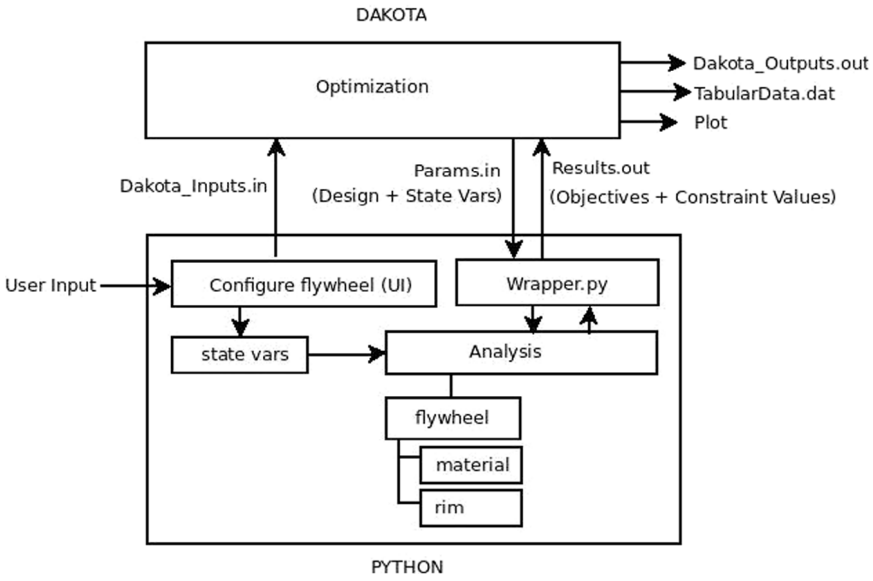

Fig. 2. Schematic of the Python-DAKOTA interface.

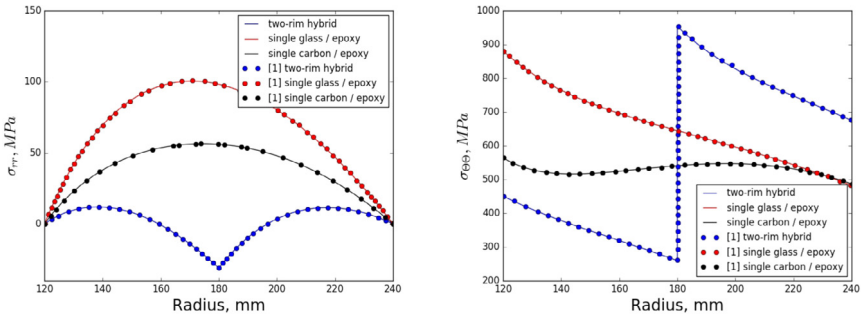

Fig. 3. Comparison of simulated and literature results (Krack et al., 2010) for (a) Radial and (b) Hoop stress distributions in 2-rim and 1-rim composite flywheels.

Table 2
Optimal glass/epoxy and carbon/epoxy composite rotors for varying cost ratios.

Optimization framework	$\frac{d_{carbon}}{d_{glass}}$	E^{opt}, MJ	ω, rpm	r^1_{out}, mm
Literature Data (Krack et al., 2010)	[11.3684–∞)	2.205	18,661	240.0
	[2.3271–11.3684)	11.387	45,363	187.18
	[0.1712–2.3271)	12.459	48,219	166.51
	[0.0–0.1712)	4.672	30,137	120.0
Simulation	20	2.212	18,692	239.99
	5	11.396	45,381	187.18
	1	12.487	48,278	166.39
	0.1	4.670	30,134	120.01

Table 3
Optimal composite rotors with different binding constraints.

Flywheel	δ^1, mm	E^{opt}, MJ	ω, rpm	r^1_{out}, mm	Binding Constraint
Glass-Epoxy, Carbon-Epoxy	0	12.486	48,278	166.39	Material failure
Kevlar49-Epoxy, Carbon-Epoxy	0.4	6.39	35,477	149.04	Material failure, Interface Stress

compressive at higher speeds, and there was no need of checking for the rim detachment constraint. This is because the ratio of the specific stiffnesses of the composite materials used in the study were very similar. Fig. 4(a) shows the feasible range of designs for the glass-epoxy and carbon-epoxy rotor used in Krack et al. (2010). It can be seen that the material failure constraint is the binding constraint, and the rim detachment constraint is non-binding. However, when there is a large difference in the specific stiffness of the 2 rims, the rim detachment constraint also tends to become a binding constraint. Fig. 4(b) shows the feasible range of designs using a kevlar-epoxy and carbon-epoxy rotor, with a press-fit interference of 0.4 mm between the rims. It is clear that there is a need to check for both constraints in the latter case. The focus of this study is to select the best flywheel materials for various performance criteria. Hence, the addition of the rim detachment constraint is important, in order to evaluate all the

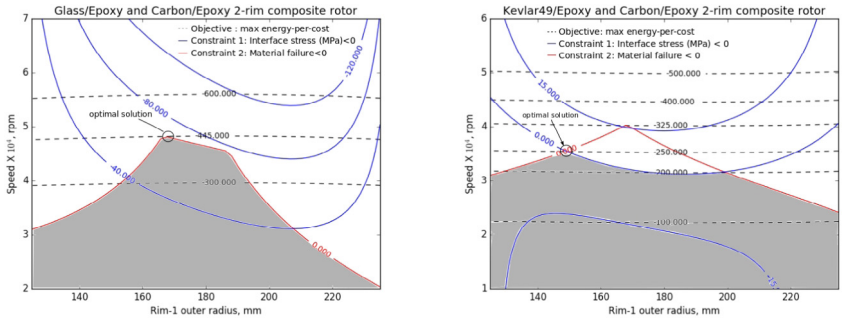

(a) (b)

Fig. 4. Rim detachment failure as a (a) non-binding constraint, and (b) binding constraint.

materials and their combinations. The optimal designs for the two flywheels evaluated in this study are also depicted in Table 3.

4. Results and discussion

The optimization problems formulated in Section 3 were solved using a set of 18 high strength metals and composites whose material properties are in Tables A.1 and A.2. The 3D material properties of the composite laminates were computed using the properties of some typical laminae in Autodesk Helius Composite software (Autodesk Helius Composite, 2017). The costs of the metals were based on current wholesale market prices. The costs of the composites were calculated using the volume fraction of the composite, along with market prices of the composite fiber rovings, and prices of the matrix materials such as resin and hardener. To alleviate the impact of the uncertainty in absolute costs on the results, all material costs were normalized with respect to the cost of the cheapest material in the evaluated set of materials before their use in the optimization problem. The cost of a rotor can depend on factors such as manufacturing process and complexity of design. However, this study only used the cost of the material, and did not account for manufacturing and other costs. Manufacturing costs vary widely with scale and therefore will not be included. A recent study by Mittelstedt et al. (2018) could be used to estimate such costs.

Krack et al. (2011a) determined the effect of the number of composite rims on the maximum energy-per-cost ratio of the rotor. They found that the objective function value did not significantly change with an increase of rims beyond two. They concluded that the increase in manufacturing complexity was not worthwhile, considering the small change in objective with increasing rims. Based on the findings from this study, the maximum number of composite rims was limited to two.

The performance criterion, or the objective function was maximized by varying a combination of the following design variables: rpm ω, and relative rim thickness, which depend on r^1_{out}. The choice of optimization objective, which was used as a performance index to compare the rotor materials, was seen to affect the optimal flywheel design. A parametric study was then conducted by varying the number of press-fit rims n and the materials used in the rims $material_j$. The number of press-fit rims, n, was limited to a maximum of 2, and a fixed rotor height of 50 mm, inner radius of 110 mm and outer radius of 200 mm were used for the study. For multi-rim rotors, the press-fit interference was fixed at 0.4 mm.

The optimization convergence criterion was defined by the DAKOTA parameters 'threshold delta', 'function precision' and 'maximum number of black-box evaluations', which were set to 10^{-6}, 10^{-10} and 1000 respectively. The 'variable neighborhood search' parameter was set to 0.5.

4.1. Post-optimality analysis

A post-optimality analysis was conducted to determine how the convergence criteria and the design variables affected the optimal solution. An optimal 1-rim metal flywheel composed of 'Stainless-Steel-455', and an optimal 2-rim composite flywheel with S2-Glass-Epoxy/IM7-8552 rims, with maximum total stored energy were chosen for this study.

The 'threshold delta' convergence parameter was found to reduce the kinetic energy by 0.15%, 0.5% and 18% when it was increased from 10^{-6} to 10^{-3}, 10^{-2} and 10^{-1} respectively. A sensitivity analysis on the 'function precision' parameter, which could be as large as the 'threshold delta' parameter established an identical effect on the optimal solution. Thus values of 'threshold delta' and 'function precision' not exceeding 10^{-3} were determined to be sufficient for the study. The optimality of the solutions was also verified by checking for KKT optimality conditions.

The optimization design variables were the operating speed and the relative thickness of rims for multi-rim rotors. A 5% reduction in the operating speed reduced the kinetic energy by nearly 10%. In case of optimal 2-rim composite rotors, the relative thickness of the rims could also affect the objective function. It was found that, the kinetic energy of an optimal S2-Glass-Epoxy/IM7-8552 rotor changed by less than 1% when the thickness of the first rim was changed by 5%. For the case where the objective improved, the material constraints were violated, which indicates that, in order to counteract the effect of manufacturing tolerances on the design, it might be necessary to lower the operating speed to prevent material failure in 2-rim rotors.

4.2. Optimal flywheels using maximum kinetic energy criterion

The kinetic energy of the flywheel was maximized and the performance of the various rotor designs is presented in Table 4. The stress distributions in the optimal 1-rim metal, 1-rim composite, 2-rim composite and 2-rim hybrid flywheels are shown in Fig. 5. The material failure constraint is a binding constraint in all the optimal designs. However, in some 2-rim rotor designs, the rim-detachment constraint also becomes a binding constraint. Some optimal 2 rim composite rotors where the rim-detachment is a binding constraint are Kevlar49-Epoxy/AS4-3501-6, AS4-8552/IM7-8551-7 and T300-BSL914C/T300-PR319.

The following observations can be made from the study:

1. The average kinetic energy of optimal 1-rim flywheels made from composite was around 1.5 times that of metal 1-rim flywheels. The kinetic energy was maximized by allowing the operating speed and inner radius of the rotor to vary. It was found that metal flywheels were around 3.7 times heavier than composites. However, composite flywheels were 4 times costlier and operated at 2.3 times the speed of metal flywheels

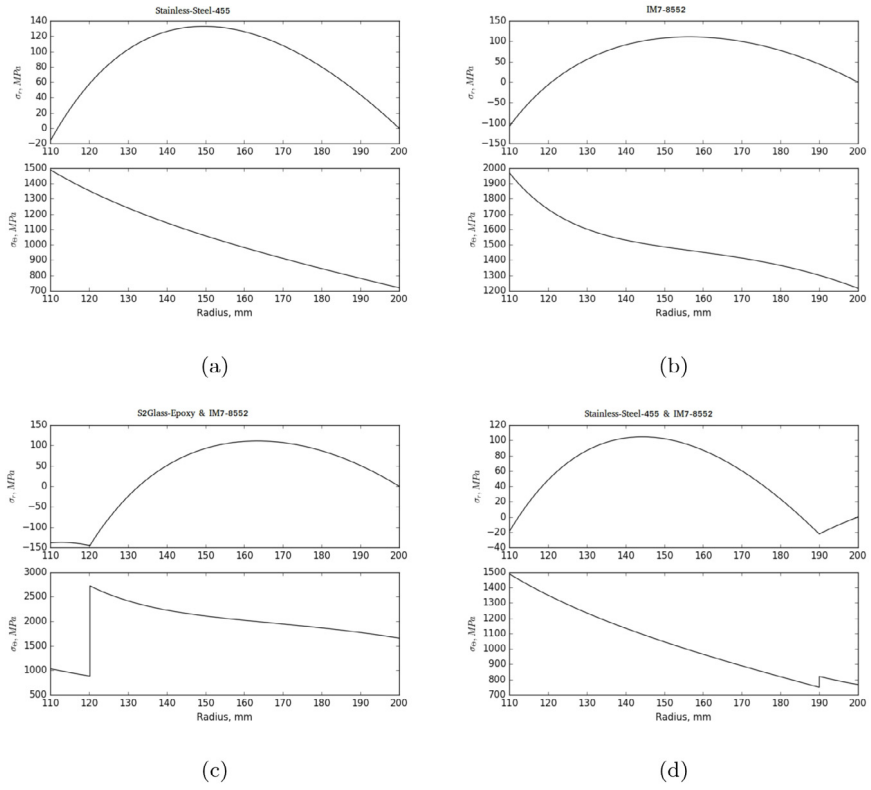

Fig. 5. Maximum kinetic energy criterion : Radial (top) and hoop (bottom) stress distributions for optimal (a) 1-rim metal, (b) 1-rim composite, (c) 2-rim composite, (d) 2-rim hybrid rotors.

Table 4
Comparison of optimal flywheel designs based on kinetic energy criterion.

Flywheel	Material	Kinetic energy, kJ	Speed, rpm	Rim radii, mm	Mass, kg	Relative cost
Metal, 1-rim	Al-6061-T6	418.86	15,713	(110–200)	11.87	27.31
Metal, 1-rim	Al-2024	637.04	19,167	(110–200)	12.13	46.61
Metal, 1-rim	Carbon-Steel-1020	685.47	11,818	(110–200)	34.35	60.47
Metal, 1-rim	Al-7075-T6	709.56	20,156	(110–200)	12.22	37.53
Metal, 1-rim	Steel-4340	749.61	12,351	(110–200)	34.40	34.40
Metal, 1-rim	Stainless-Steel-15–7	1180.80	15,682	(110–200)	33.61	90.42
Metal, 1-rim	Steel-18Ni-300	1203.03	15,460	(110–200)	35.23	53.91
Metal, 1-rim	Stainless-Steel-440C	1947.44	20,100	(110–200)	33.74	42.51
Metal, 1-rim	Stainless-Steel-455	2369.82	22,087	(110–200)	34.00	78.21
Composite, 1-rim	T300-BSL914C	786.48	28,388	(110–200)	6.83	216.65
Composite, 1-rim	Kevlar49-Epoxy	885.49	31,970	(110–200)	6.06	164.37
Composite, 1-rim	E-Glass-Epoxy	1060.36	28,565	(110–200)	9.09	170.31
Composite, 1-rim	S2-Glass-Epoxy	1355.19	32,958	(110–200)	8.73	269.97
Composite, 1-rim	AS4-3501–6	1360.29	36,957	(110–200)	6.97	185.68
Composite, 1-rim	T300-PR319	1403.14	37,877	(110–200)	6.84	217.12
Composite, 1-rim	AS4–8552	2404.63	49,343	(110–200)	6.91	184.54
Composite, 1-rim	IM7-8551–7	2452.16	49,883	(110–200)	6.89	246.78
Composite, 1-rim	IM7–8552	3150.50	56,292	(110–200)	6.96	248.98
Composite, 2-rim	EGlass-Epoxy, IM7-8551–7	3154.54	56,263	(110–119.32–200)	7.06	240.92
Composite, 2-rim	EGlass-Epoxy, AS4–8552	3224.14	56,740	(110–120.48–200)	7.10	183.31
Composite, 2-rim	Kevlar49-Epoxy, T300-BSL914C	2213.79	48,459	(110–155.64–200)	6.49	193.93
Composite, 2-rim	Kevlar49-Epoxy, AS4-3501–6	2532.95	51,162	(110–146.72–200)	6.66	178.48
Composite, 2-rim	Kevlar49-Epoxy, IM7-8551–7	3716.71	61,814	(110–134.25–200)	6.72	229.28
Composite, 2-rim	S2-Glass-Epoxy, AS4-3501–6	2798.60	52,233	(110–133.60–200)	7.33	203.05
Composite, 2-rim	S2-Glass-Epoxy, IM7–8552	4072.10	63,650	(110–120.22–200)	7.11	250.75
Composite, 2-rim	AS4-8552, IM7-8551–7	3302.65	57,882	(110–137.42–200)	6.90	231.64
Composite, 2-rim	T300-BSL914C, T300-PR319	1738.68	42,169	(110–134.62–200)	6.84	217.01
Hybrid, 2-rim	Al-6061-T6, Kevlar49-Epoxy	441.64	17,006	(110–190–200)	11.06	46.47
Hybrid, 2-rim	Al-2024, IM7–8552	719.87	21,325	(110–190–200)	11.41	74.90
Hybrid, 2-rim	Steel-4340, IM7–8552	760.70	13,598	(110–190–200)	30.56	64.39
Hybrid, 2-rim	Stainless-Steel-15-7, T300-PR319	1153.48	16,937	(110–190–200)	29.87	108.13
Hybrid, 2-rim	Stainless-Steel-440C, Kevlar49-Epoxy	1804.94	21,208	(110–190–200)	29.87	59.55
Hybrid, 2-rim	Stainless-Steel-455, Kevlar49-Epoxy	2188.32	23,265	(110–190–200)	30.10	90.26
Hybrid, 2-rim	Stainless-Steel-455, IM7–8552	2274.63	23,644	(110–190–200)	30.22	102.08

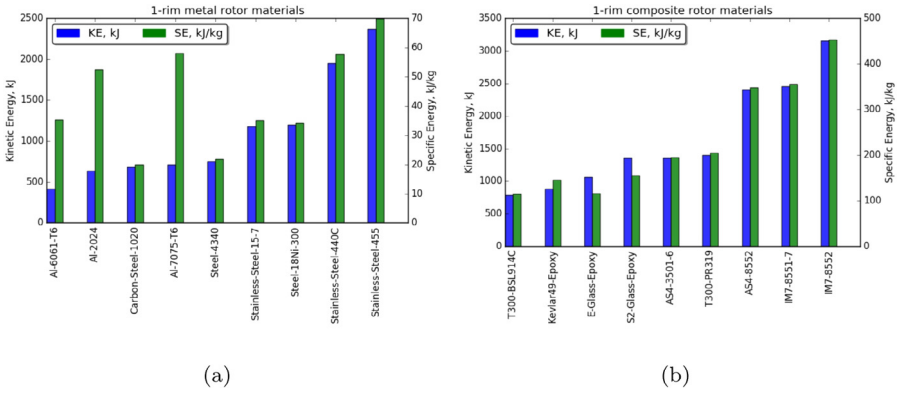

(a) (b)

Fig. 6. Comparison of kinetic energy and specific energy of (a) Metal, (b) Composite rotor materials.

2. The kinetic energy of composite flywheels could be increased by using 2 press-fit composite rims instead of 1. The rims were chosen in increasing order of stiffness along the radius. This method allowed the kinetic energy to increase by up to 150%, accompanied by an increase in the operating speed. A similar study was conducted by Ha et al. (2008), where Graphite/Epoxy rotors with 1 to 5 rims were optimized by varying the thickness and interference of the press-fit rims. It was found that increasing the number of rims from 1 to 2 could increase the specific energy of the rotor by 145%.
3. The use of 2 press-fit metal rims resulted in a trivial 1-rim solution.
4. The use of more than 2 composite-rim rotors could further improve the kinetic energy, but the increase was not large enough to justify the use of multiple rims, which would need a more complex manufacturing process.
5. All the above designs used a constant height rotor, corresponding to a shape factor of 0.5. Practically, metal flywheels can be fabricated with better shape factors, and thus, can store more kinetic energy than projected in these simulation results. Thus the use of rotor shape and topology as a design variable needs to be explored.
6. Burst failure is one of the main causes of concern while using metal flywheels, which fail in few, large fragments, whereas; composites fail either by delamination or due to the fibers breaking into small fragments (Genta, 2014). Thus, the containment structure for composite flywheels must be designed to avoid fragment penetration, whereas, that of metal flywheels must restrict the forces or moments of the flywheel fragments from being transferred outside. To address the concern of burst safety, a hybrid metal-composite press-fit rotor was also optimized in this study. The outer composite rim had a fixed thickness of 10 mm, and was primarily for safety. The flywheel was then optimized, by allowing the rpm of the rotor to vary. It was found that the kinetic energy was nearly the same as that of 1-rim metal flywheels, with a marginal increase in the cost and operating speeds. These hybrid flywheels also provide an opportunity to optimize the shape of the inner metallic rim, which could further increase the kinetic energy and reduce the mass and the cost of the rotor.
7. The effect of using material specific, multi-axial failure criteria was also studied. It was found that, when the optimal 1-rim composite rotor was designed using the multi-axial Tsai–Wu failure criterion instead of the maximum stress criterion, there was a nearly 2% reduction in the kinetic energy of the rotor. Similarly, when the optimal 1-rim metal rotor was designed using the von Mises stress criterion, there was almost no change in the performance, as compared to the original design. Thus, for 1-rim rotors, the effect of failure criterion on the comparative study could be neglected. However, in the case of an optimal 2-rim composite rotor, a change in the failure criterion (from maximum stress to Tsai–Wu) reduced the performance of an optimal 2-rim composite rotor by around 25%, as the shape of the binding constraints had changed considerably. Thus, the design and performance of multi-rim composite rotors could be affected significantly by the choice of failure criterion, with the maximum stress failure criterion used over-predicting the performance.

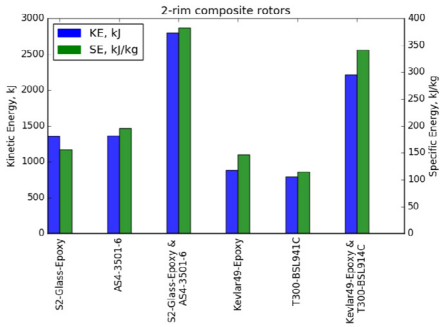

Fig. 7. Comparison of kinetic energy and specific energy of optimal 2-rim and 1-rim rotors.

4.3. Optimal flywheels using maximum specific energy criterion

The specific energy of the flywheel was maximized, and a comparison of the performance of various rotor designs is presented in Figs. 6 and 7. The material failure constraint is a binding constraint in all the optimal designs. However, in some 2-rim rotor designs, the rim-detachment constraint also becomes a binding constraint. Some optimal 2 rim composite rotors where the rim-detachment is a binding constraint are Kevlar49-Epoxy/AS4-3501-6, AS4-8552/IM7-8551-7 and T300-BSL914C/T300-PR319.

The following observations can be made from the study:

1. The average specific energy of optimal 1-rim composite flywheels was 5–6 times that of optimal 1-rim metal flywheels.
2. The specific energy of rotors made from isotropic metals was in the range 6–19 Wh/kg, and that of composite rotors was in the range 32–126 Wh/kg. The specific energy of composite flywheels was significantly lower than the theoretical maximum specific energy of the materials previously reported in literature. For example, Genta (2014) reported the specific strengths of Aluminium Alloy 2024 and unidirectional

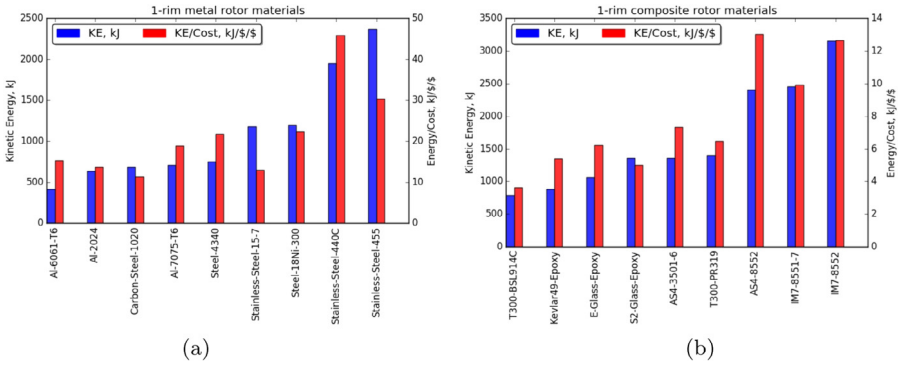

Fig. 8. Comparison of kinetic energy and specific energy of (a) Metal, (b)Composite rotor materials.

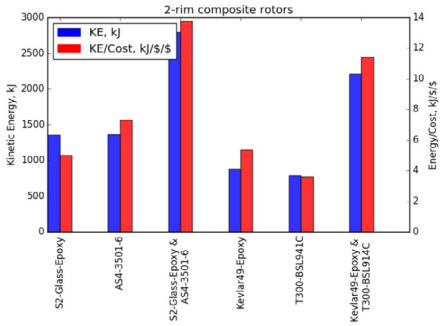

Fig. 9. Comparison of kinetic energy and energy per cost of optimal 2-rim and 1-rim rotors.

Kevlar composite as 46 and 240 Wh/kg respectively. Assuming a shape factor of 0.303 corresponding to an annular constant thickness disk, the flywheels made from these materials would have theoretical specific energies of 13.938 and 72.72 Wh/kg respectively. The corresponding optimal flywheels using these materials resulted in specific energies of 14.58 and 37.26 Wh/kg. This justified the need for an optimization formulation and a rotor model that captures the physical and material failure constraints on the rotor.

3. The specific energy of composite rotors could be improved by up to 150% over 1-rim rotors, by using multiple press-fit rims.

4.4. Optimal flywheels using maximum energy per cost criterion

The energy-per-cost of the flywheel was maximized and a comparison of the performance of various rotor designs is presented in Figs. 8 and 9. The material failure constraint is a binding constraint in all the optimal designs. However, in some 2-rim rotor designs, the rim-detachment constraint also becomes a binding constraint. Some optimal 2 rim composite rotors where the rim-detachment is a binding constraint are Kevlar49-Epoxy/AS4-3501-6, AS4-8552/IM7-8551-7 and T300-BSL914C/T300-PR319.

The following observations can be made from this study:

1. The average energy-per-cost of optimal 1-rim metal flywheels was 2.7 times that of optimal 1-rim composite flywheels.
2. The use of 2 press-fit composite rims increased the energy-per-cost of the composite rotor, but not enough to be competitive with high strength 1-rim metal rotors of the same dimensions.

5. Conclusions

This article optimized 1-rim and 2-rim flywheel rotors made of various metal and composite materials to determine the optimal rotor material. It was found that the choice of optimal material depended on the performance criterion being used. Composite rotors performed better in terms of specific energy, whereas metal rotors had a better energy per cost. The total kinetic energy of both composite and metal rotors of a constant thickness were comparable. It was also shown that the specific energy of the composite rotors was significantly lower than the theoretical specific energy of the rotor materials, which only used tensile material failure considerations. Thus, the significance of material failure and other physical constraints was established. The optimization model allowed us to apply constraints on the radial stresses, as well as direction-dependent failure modes, which limited the practically achievable specific energy of orthotropic materials such as composites used to construct flywheel rotors.

The means of improving the performance of the flywheels were studied, and it was shown that press-fitted multi-rim composite rotors with specific material sequences could outperform single rim composite and metal flywheels, in terms of total energy or specific energy. However, when energy-per-cost was used as the performance criterion, 2-rim rotors offered no significant advantage over 1-rim rotors. Further improvements in the performance of metal flywheels can be achieved by optimizing the stress distributions, using variations in the shape or topology of the rotor; however, this analysis would need a 2D or 3D numerical rotor model. The effect of fatigue on the effective performance of the different types of flywheel rotors over their expected lifetimes could also contribute to the choice of rotor material and needs to be studied.

Acknowledgment

The authors acknowledge the Natural Sciences and Engineering Research Council of Canada Energy Storage Technology (NEST) Network for financial assistance.

Appendix. Material properties

The material properties of the metals and composites used in the flywheel rotors designed in this study can be found in Tables A.1 and A.2. The relative cost of each material is determined by normalizing the cost of the material with respect to the cost of the cheapest material in the evaluated set of materials.

Table A.1
Isotropic material properties (Ledbetter, 1982).

Material	E GPa	G GPa	ν	ρ g/cm^3	Yield strength MPa	Relative cost /kg
Al-2024	73.1	27.1	0.332	2.77	417.8	3.84
Al-6061-T6	69.6	26.3	0.331	2.71	275	2.30
Al-7075-T6	71.8	26.8	0.33	2.79	465	3.07
Steel-4340	205.0	76.5	0.29	7.85	470	1.0
Steel-18Ni-300	190.0	66.3	0.318	8.04	758	1.53
Stainless-Steel-15–7	201.0	77.9	0.32	7.67	745	2.69
Stainless-Steel-440C	203.0	93.1	0.284	7.7	1220	1.26
Stainless-Steel-455	197.9	75.8	0.3	7.76	1489	2.30
Carbon-Steel-1020	206.2	80.0	0.288	7.84	429.6	1.76

Table A.2
Composite material properties (Autodesk Helius Composite, 2017).

Material	V_f	E_θ GPa	E_r GPa	$G_{\theta r}$ GPa	G_{rz} GPa	$\nu_{\theta r}$	ν_{rz}	ρ g/cm^3	$\sigma^{ult}_{\theta,T}$ MPa	$\sigma^{ult}_{\theta,C}$ MPa	$\sigma^{ult}_{r,T}$ MPa	$\sigma^{ult}_{r,C}$ MPa	$\tau^{ult}_{\theta r}$ MPa	relative cost /kg
AS4-3501–6	0.6	127	11.15	6.55	3.64	0.27	0.53	1.591	1950	1480	48	200	79	26.63
AS4–8552	0.58	135.1	9.63	4.95	3.35	0.30	0.43	1.577	2206	1531	80	259.9	114.5	26.69
E-Glass Epoxy	0.45	44.81	12.41	5.51	3.59	0.28	0.36	2.076	1035	620	48	137.8	68.9	18.72
IM7-8551–7	0.6	165.8	8.56	5.59	2.94	0.27	0.46	1.574	2560	1590	73	185	90	35.77
IM7–8552	0.57	139.7	11.39	4.75	3.89	0.32	0.46	1.588	2723	1689	111	215.9	119.9	35.77
Kevlar-49 Epoxy	0.45	75.84	5.51	2.06	1.54	0.34	0.47	1.384	1378	275	29	137.8	62	27.10
S-2 Glass Epoxy	0.45	55.84	17.92	6.20	3.89	0.27	0.35	1.993	1999	965	62	155	93	30.91
T300-BSL914C	0.6	138.1	11	5.43	3.57	0.28	0.54	1.559	1500	900	27	200	80.0	31.71
T300-PR319	0.6	128.9	5.706	1.33	1.84	0.32	0.55	1.562	1378	950	40	125	97	31.71

References

ABB Powerstore Webpage, https://library.e.abb.com/public/e13f1d26d87e9167c1257c37002e38bf/9AKK100580A2551_Powerstore_Brochure_EN_HR_(Dic2013).pdf. (Accessed 7 July 2017).

ActivePower Webpage, http://www.activepower.com/en-US. (Accessed 7 July 2017).

Adam, B., Bauman, L., Bohnhoff, W., Dalbey, K., Ebeida, M., et al., 2015. Dakota, a multilevel parallel object-oriented framework for design optimization, parameter estimation, uncertainty quantification, and sensitivity analysis: Version 6.0 user manual. In: Tech. Rep.. Sandia National Laboratories.

Amber Kinetics Webpage, http://amberkinetics.com/. (Accessed 7 July 2017).

Arani, A.K., Karami, H., Gharehpetian, G., Hejazi, M., 2017. Review of flywheel energy storage systems structures and applications in power systems and microgrids. Renew. Sustain. Energy Rev. 69, 9–18.

Arnold, S., Saleeb, A., Al-Zoubi, N., 2002. Deformation and life analysis of composite flywheel disk systems. Composites B 33 (6), 433–459.

Audet, C., Béchard, V., Le Digabel, S., 2008. Nonsmooth optimization through mesh adaptive direct search and variable neighborhood search. J. Global Optim. 41 (2), 299–318.

Autodesk Helius Composite, https://knowledge.autodesk.com/support/helius-composite/learn-explore/caas/CloudHelp/cloudhelp/2015/ENU/ACMPDS/files/GUID-2B4538D7-227F-4C9F-891F-785F90CA10CA-htm.html. (Accessed 1 November 2017).

Beacon Power Webpage, http://beaconpower.com/carbon-fiber-flywheels/. (Accessed 7 July 2017).

Bitterly, J.G., 1998. Flywheel technology: Past, present, and 21st century projections. IEEE Aerosp. Electron. Syst. Mag. 13 (8), 13–16.

Calnetix Webpage, https://www.calnetix.com/. (Accessed 7 July 2017).

Cardenas, R., Pena, R., Asher, G., Clare, J., 2001. Control strategies for enhanced power smoothing in wind energy systems using a flywheel driven by a vector-controlled induction machine. IEEE Trans. Ind. Electron. 48 (3), 625–635.

Daoud, M.I., Massoud, A.M., Abdel-Khalik, A.S., Elserougi, A., Ahmed, S., 2016. A flywheel energy storage system for fault ride through support of grid-connected VSC HVDC-based offshore wind farms. IEEE Trans. Power Syst. 31 (3), 1671–1680.

Energiestro Webpage, http://www.energiestro.net/. (Accessed 7 July 2017).

Ertz, G., 2014. Development, manufacturing and testing of a multi-rim (hybrid) flywheel rotor.

Genta, G., 2014. Kinetic Energy Storage: Theory and Practice of Advanced Flywheel Systems. Butterworth-Heinemann.

Ha, S.K., Han, H.H., Han, Y.H., 2008. Design and manufacture of a composite flywheel press-fit multi-rim rotor. J. Reinf. Plast. Compos. 27 (9), 953–965.

Krack, M., Secanell, M., Mertiny, P., 2010. Cost optimization of hybrid composite flywheel rotors for energy storage. Struct. Multidiscip. Optim. 41 (5), 779–795.

Krack, M., Secanell, M., Mertiny, P., 2011a. Advanced optimization strategies for cost-sensitive design of energy storage flywheel rotors. J. Adv. Mater. 43 (2), 65–78.

Krack, M., Secanell, M., Mertiny, P., 2011b. Cost optimization of a hybrid composite flywheel rotor with a split-type hub using combined analytical/numerical models. Struct. Multidiscip. Optim. 44 (1), 57–73.

Krack, M., Secanell, M., Mertiny, P., 2011c. Rotor design for high-speed flywheel energy storage systems. In: Energy Storage in the Emerging Era of Smart Grids. InTech.

Ledbetter, H., 1982. Physical Properties Data Compilations Relevant to Energy Storage. National Bureau of Standards.

LEVISYS Webpage, http://www.levisys.com/en/technologie.html. (Accessed 7 July 2017).

Liu, H., Jiang, J., 2007. Flywheel energy storage—an upswing technology for energy sustainability. Energy Build. 39 (5), 599–604.

Mittelstedt, M., Hansen, C., Mertiny, P., 2018. Design and multi-objective optimization of fiber-reinforced polymer composite flywheel rotors. Appl. Sci. 8 (8), 1256.

Piller Webpage, http://www.piller.com/en-GB/205/energy-storage. (Accessed 7 July 2017).

Powerthru Webpage, http://www.power-thru.com/. (Accessed 7 July 2017).

Silva-Saravia, H., Pulgar-Painemal, H., Mauricio, J.M., 2017. Flywheel energy storage model, control and location for improving stability: The chilean case. IEEE Trans. Power Syst. 32 (4), 3111–3119.

Stornetic GmBH Webpage, http://stornetic.com/. (Accessed 7 July 2017).

Temporal Power Webpage, http://temporalpower.com/. (Accessed 7 July 2017).